An approach to consider the arterial residual stresses in modelling of a patient-specific artery

Janez Urevc[1], Miroslav Halilovič[1], Milan Brumen[2,3] and Boris Štok[1]

Abstract
In this work, the residual stress state of a human common carotid artery is predicted using the so-called thermomechanical analogy approach. The purpose of the approach is to enable consistent mapping of residual stresses and the respective configuration from a circular arterial segment to a patient-specific arterial geometry. This is achieved by applying proper volumetric dilatations to the actual arterial stress-free in vivo geometry, which makes use of the analogy that states that the bending stresses can be obtained on an equivalent manner by applying proper thermal dilatations. The common carotid artery data are obtained in vivo from a healthy 28-year-old man using non-invasive methods. The predicted residual stresses of the common carotid artery are in good quantitative agreement with the data from prior work in this field. The approach is validated by predicting the common carotid artery zero-stress state configuration, where a sector-like (cut-open) state is obtained. With this approach, it is thus possible to predict the residual stresses as well as the configuration of patient-specific arterial geometry without the need to model its cut-open zero-stress configuration.

Introduction

The mechanical environment and the properties of arteries play an important role in the origin and progression of vascular diseases.[1] Numerical simulations of arterial mechanical response can therefore help us to understand the role of the arterial in vivo mechanical response in vascular pathogenesis. Additionally, it can aid in the improvement of (non)surgical procedures and the development of prosthetic materials and tissue equivalents.[1] However, one of the major challenges in vascular biomechanics that has not yet been solved sufficiently is the prediction of a patient-specific arterial stress-free state (or any intermediate arterial stress state and its corresponding configuration).

Experimental observations show that the geometry of the arterial zero-stress state assumes a sector-like shape.[2–4] This phenomenon is associated with the fact that the arterial unloaded state, that is, a state when the artery is removed from the body, is pre-stressed. It is believed that these stresses, known as *residual stresses*, homogenise the circumferential stress when the artery is under physiological pressure.[5,6] Residual stresses can be measured experimentally with the so-called opening

[1]Laboratory for Numerical Modelling and Simulations, Faculty of Mechanical Engineering, University of Ljubljana, Ljubljana, Slovenia
[2]Faculty of Medicine, University of Maribor, Maribor, Slovenia
[3]Jožef Stefan Institute, Ljubljana, Slovenia

Corresponding author:
Janez Urevc, Laboratory for Numerical Modelling and Simulations, Faculty of Mechanical Engineering, University of Ljubljana, Aškerčeva 6, 1000 Ljubljana, Slovenia.
Email: janez.urevc@fs.uni-lj.si

angle method, introduced by Chuong and Fung.[5] In the experiment, a longitudinal cut is performed on a dissected arterial ring. Because the ring is pre-stressed, it opens up, and the amount of the opening is then used as a measure of residual stress. For an in vivo assessment of residual stresses, an approach proposed by Takamizawa and Hayashi[7] is normally used. They assumed that the intraluminal distribution of circumferential stresses under a physiological loading condition is uniform, which can be achieved only with the existence of (bending) residual stresses. However, the approach, known as the *uniform strain hypothesis*, appears to be applicable only for idealised (circular) arterial rings[8] and can hardly be used for a complex three-dimensional (3D) arterial geometry.

Several approaches can be found in the literature for predicting the arterial residual stress state. Alastrué et al.[6] used a multiplicative split of the deformation gradient tensor into a non-compatible tensor, which takes into account the initial strain field, and an elastic compatible tensor, which results from the compatibility enforcement. The first is obtained from the opening angle experiment by computing the residual stress of a circular arterial ring, whereas the latter basically maps the obtained state onto an equilibrium state. In Polzer et al.,[8] an algorithm is proposed that leads to the prediction of residual stresses through volumetric tissue growth. Residual strains are iteratively applied to an arterial configuration with the aim of satisfying the homogeneous stress hypothesis at the mean arterial pressure load. However, the arterial configuration used, based on which the residual stresses are applied to, needs to be initially given. Zhou and Lu[9] proposed an inverse elastostatic formulation approach to predict the open stress-free arterial configuration inversely. This is achieved by assuming that the in vivo arterial state is under a uniform homeostatic stress throughout the thickness of the entire arterial wall. The value of the applied stress is obtained by analysing a circular arterial segment and using the opening angle as a measure of residual stress. By solving an inverse boundary value problem, the open arterial configuration can then be predicted. Schröder and Brinkhues[10] analysed gradients of suitable invariant stress measures in the thickness direction of the arterial wall. By smoothing these gradients between the inner and outer margins of individual arterial layers using their volumetric mean values, the residual stresses are obtained. This is performed by dividing the artery into suitable radial sections on which the smoothing condition is enforced independently. Additionally, different growth theories have been introduced to predict how residual stresses develop over time and, also, at different length scales.[11–13] However, they have been mostly presented by treating an idealised arterial ring.

In this work, the residual stress state of a human common carotid artery (CCA) is numerically predicted using the thermomechanical analogy (TMA) approach. The approach, which was recently proposed by the authors[14] and is, in this work, applied to model the response of a human CCA for the first time, predicts the arterial residual stress state by applying proper volumetric dilatations to the arterial in vivo stress-free configuration. The amount of dilatation required is obtained by characterising the mechanical response of an idealised (circular) arterial ring, and the opening angle method is used to quantify the residual stress. The CCA data are obtained from a 28-year-old healthy male using non-invasive methods. The mechanical response of the artery is, in this work, treated in a simplified manner as hyperelastic and isotropic. The approach is validated by comparing the predicted CCA residual stresses with the data of residual stresses available in the literature and by predicting the CCA cut-open zero-stress state.

The structure of this article is as follows. First, the TMA approach is presented in a general manner in order to highlight its main steps and their purposes. The experimental data and their acquisition are then briefly presented in section 'Experimental data'. In section 'Modelling the CCA mechanical response', the TMA approach is then applied to the analysed CCA, whereas sections 'Results and discussion' and 'Conclusion' give the results and conclusions, respectively.

The general concept of using the TMA approach

Let us first present the general concept of the TMA approach using a case of treating a bended and axially stretched cantilever beam, presented in Figure 1(a). Although this example is in no direct relation with the problem of observing an arterial section per se, it will highlight all the key steps of the methodology in a somewhat simple and easy-to-understand example.

Additionally, this example demonstrates the purpose of using TMA more clearly. The general concept of applying TMA to treat an arterial segment is then presented in section 'Applying the TMA approach to predict the mechanical response of an arterial segment'.

Bended and axially stretched beam example

We can observe the beam in Figure 1(a) in its final configuration Ω_2. The beam has a rectangular cross-sectional area with a variable height $h_2(x)$ and variable longitudinal curvature. In Figure 1(a), three configurations are presented: the zero-stress state Ω_0; the configuration where the beam is subjected to residual stresses $\Omega_{1\lambda}$ and the loaded configuration Ω_2. For the beam, we
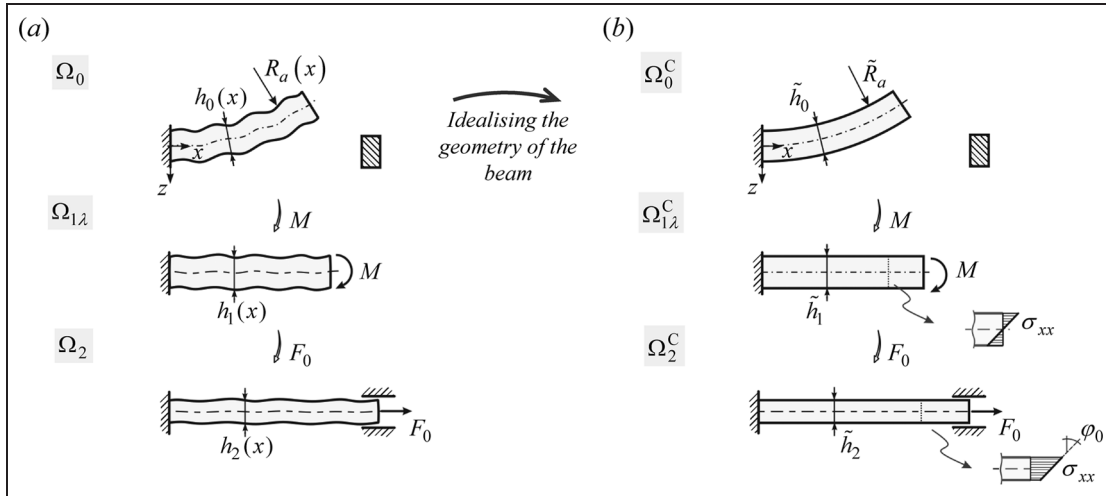
Figure 1. Bended and axially stretched beam example: (a) the observed problem and (b) beam with idealised geometry.

want to predict the stresses in its loaded state Ω_2, while the initial zero-stress configuration of the beam Ω_0 is unknown because the residual stresses are also not known. The known data in this problem are the configuration of the beam in its loaded state Ω_2 and the value of the force, F_0, which stretches the beam from $\Omega_{1\lambda}$ to Ω_2. The material of the beam is assumed to be incompressible and linearly elastic with the known value of Young's modulus, E_0.

The strategy for solving the presented problem is as follows. The problem is treated, first, by simplifying (idealising) the geometry of the beam into a beam with a constant height $\tilde{h}$ and uniform longitudinal curvature $\tilde{R}_a$ (Figure 1(b)). In step 2, the stresses for all configurations in Figure 1(b) can then be determined. Next, in the third step, the task is to map the stresses obtained for the idealised beam (Figure 1(b)) onto the real beam (Figure 1(a)).

However, this mapping is not trivial and has to be done accordingly. If the stresses are simply scaled from the idealised to the real geometry, the real beam might not be in static equilibrium. In this work, the TMA approach is used for the consistent mapping of stresses (step 3).

Based on the above-stated steps, we divide the process of using the TMA approach to determine the stresses in the real beam into the following three steps:

Step 1: establish the ideal case problem from the original real case problem.
Step 2: solve the corresponding ideal case problem.
Step 3: determine the mechanical response for the original real case problem by mapping the solution for the ideal case problem onto it.

Although step 3 is simply referred to as 'mapping of the ideal case problem solution', several specific activities are performed, which can be further divided into three main parts:

Sub-step 3.1: build a thermomechanical analogue (TMA) (or mapping) model for the ideal case.
Sub-step 3.2: assess the stress state on the real case geometry using the derived TMA model.
Sub-step 3.3: assess the original problem solution based on the stress state obtained in sub-step 3.2.

In the following sub-sections, the individual steps of the methodology for solving the beam problem are presented in more detail. The emphasis is mostly placed on presenting step 3.

Introduction and assumptions of the beam example. As stated, let us observe the beam in Figure 1(a). The goal is to predict the stresses and geometry for all the configurations of the beam in Figure 1(a). We know that in the loaded state Ω_2, the beam is subject to the axial force F_0. The geometry of the configuration Ω_2 and the magnitude of the force F_0 are known. By removing F_0, the beam shrinks in the axial (x) and transversal (z) directions, and the configuration $\Omega_{1\lambda}$ is obtained. Configuration $\Omega_{1\lambda}$ is not stress-free because unknown residual (bending) stresses are still present. By releasing them, the beam takes a curved zero-stress configuration Ω_0.

To summarise, the mechanical response of the observed beam cannot be determined (computed) because the initial zero-stress configuration and the residual stresses of the beam are not known.

Idealising the geometry of the beam, steps 1 and 2. In order to obtain an approximate estimation of the mechanical response of the beam, the geometry of the beam is idealised, step 1 (Figure 1(b)). This assumes that the

longitudinal axis of the beam in its loaded state Ω_2^C is a straight line, and that the height of the beam is constant $h_2(x) = \tilde{h}_2$. The idealisation further implies that the initial zero-stress geometry Ω_0^C of the beam has a single curvature with radius $\tilde{R}_a$. Therefore, in order to determine the mechanical response of the idealised beam, the only data that need to be obtained is the radius $\tilde{R}_a$.

From the elastic beam theory, it is known that the stress distribution is linear. Radius $\tilde{R}_a$ is obtained by taking additional experimental knowledge into account. Namely, let us assume that the experimental data of the beam problem show that the angle of stress distribution in the loaded state of the beam has the value φ_0 (Figure 1(b)). We will call this a hypothesis of *known stress distribution*. (As mentioned, it is presumed that this is a well-known hypothesis of the observed beam problem, similar to the *uniform strain hypothesis* in arteries, where $\varphi_0 = 0$ for circumferential stresses at the mean blood pressure. Note that in beam problem, a 'strain hypothesis' could also be used (to make the example more similar to the arterial problem – see section 'Applying the TMA approach to predict the mechanical response of an arterial segment'). 'Stress hypothesis' was chosen due to a more representative distribution of bending stresses which are easier to visualise and are probably closer to a common reader). Using this hypothesis, the initial radius $\tilde{R}_a$ of the beam can easily be determined. The height of the beam in its zero-stress state follows from the incompressibility condition. Based on this result, the mechanical response of all configurations in Figure 1(b) can be determined, which completes step 2.

The problem that arises now is how to map the mechanical response of an idealised beam (i.e. from states Ω_2^C or $\Omega_{1\lambda}^C$) onto the beam with real geometry (Figure 1(a)). For this purpose, the TMA approach, which is presented in the following, will be used.

TMA for obtaining bending stresses, step 3. The purpose of the analogy is to determine the state of the beam $\Omega_{1\lambda}^C$ (Figure 1(b)) without the bending procedure. From the field of thermomechanics, we know that the state $\Omega_{1\lambda}^C$ (i.e. its configuration and stresses) can also be determined by enforcing thermal (volumetric) dilatation in a clamped–clamped beam, as presented in Figure 2(b). More specifically, by exposing the beam Ψ_0^C in Figure 2(b) to a temperature difference ΔT_a and ΔT_b (applied to its upper and lower surfaces), the same distribution of stresses as in the $\Omega_{1\lambda}^C$ state can be obtained (Figure 2(a)). The cross-sectional temperature field in the Ψ_1^C state follows from solving a steady-state heat exchange problem where, for the present problem, a linear temperature distribution is obtained. In the following, we will refer to the thermally loaded model as a thermomechanical (TM) or fictitious model.
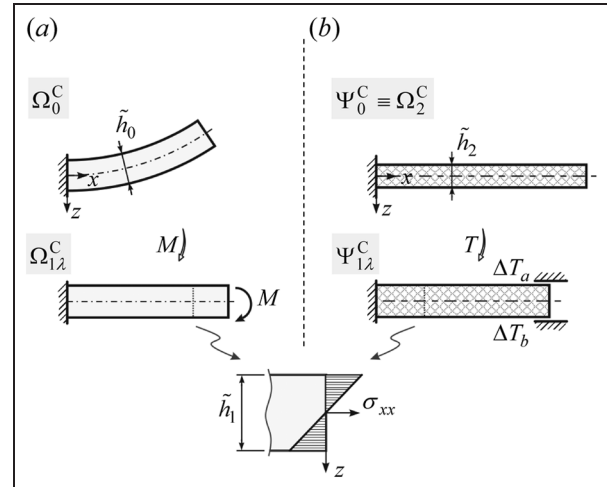
Figure 2. The stresses in the beam configuration $\Omega_{1\lambda}^C$ are obtained by (a) bending an initially curved beam Ω_0^C and (b) enforcing thermal (volumetric) dilatation on a clamped–clamped (thermomechanical) beam Ψ_0^C.

There are two benefits to such an approach. First, the bending procedure is avoided and replaced by enforcing volumetric dilatations. Second, the TM model is a fictitious model, and therefore, its initial geometry can be chosen arbitrarily. However, the material properties and the thermal loading need to be determined accordingly, as will be presented in the following sub-section.

Since we can define the initial geometry of the TM model Ψ_0^C arbitrarily, we choose it to be the same as the geometry of the beam in its loaded state Ω_2^C. This is beneficial because this is the only geometry that is initially given in the beam problem (as is also the case in treating patient-specific arteries).

Determining the properties of the TM beam model, sub-step 3.1. As mentioned, in order to apply the TMA approach, the properties of the fictitious TM model need to be determined first. Since the mechanical response of the idealised beam in Figure 1(b) has already been determined (section 'Idealising the geometry of the beam, *steps 1 and 2*'), we will use its $\Omega_{1\lambda}^C$ configuration to calibrate the properties of the TM model.

So, the aim now is to determine the properties of the idealised TM model Ψ_0^C in such a way that its loaded state $\Psi_{1\lambda}^C$ (i.e. its stresses and configuration) will match the state of the idealised beam $\Omega_{1\lambda}^C$. Let us emphasise again that the TM model merely represents a mathematical or an auxiliary model. The properties of the TM model – its loading and its material properties – have no relation to the observed beam problem per se.

The parameters that define the TMA beam are the thermal loadings ΔT_a and ΔT_b and the material

properties, which are Young's modulus E^{Ψ} and the coefficients of thermal expansion in the axial α_x and transverse α_z directions of the beam (Figure 3(a)). Because the initial Ψ_0^C and the final geometry $\Psi_{1\lambda}^C$ of the TMA beam are both prescribed, the strains in the longitudinal and transverse directions are also prescribed. Since in general they differ, this can be satisfied by the orthotropic properties of the thermal expansion coefficient α.

Altogether, this defines up to five unknown parameters (ΔT_a, ΔT_b, E^{Ψ}, α_x and α_z). They follow from the mathematical solution of the problem, which is briefly presented in the following.

Since the initial Ψ_0^C and the final $\Psi_{1\lambda}^C$ geometry of the beam are prescribed, the dilatation of the beam's neutral axis $\tilde{L}_1 - \tilde{L}_2$ (Figure 3(a)) and the dilatation of the beam's height $\tilde{h}_1 - \tilde{h}_2$ are known. From the theory of linear elasticity, the following equation can be obtained

$$\begin{aligned} \tilde{L}_1 - \tilde{L}_2 &= \alpha_x \Delta \tilde{T} \tilde{L}_2 \\ \tilde{h}_1 - \tilde{h}_2 &= \alpha_z \Delta \tilde{T} \tilde{h}_2 \end{aligned} \quad (1)$$

where $\Delta \tilde{T}$ is the mean value of the temperature loading $\Delta \tilde{T} = 0.5(\Delta T_a + \Delta T_b)$. Furthermore, the relation to the beam's internal bending moment M follows from the Euler–Bernoulli equation

$$M(x) = -E^{\Psi} I_y \left(\frac{\mathrm{d}^2 w(x)}{\mathrm{d}x^2} + \alpha_x \frac{\Delta T_b - \Delta T_a}{\tilde{h}_2} \right) \quad (2)$$

where I_y is the second moment of area. Because the beam does not deflect $w''(x) = 0$, it follows that $M(x) = $ const. The cross-sectional distribution of the beam's bending (axial) stress σ_{xx} is given by

$$\sigma_{xx}(z) = \frac{M}{I_y} z \quad (3)$$

Since the distribution of stresses in the targeting configuration $\Omega_{1\lambda}^C$ is known, being $\sigma_{xx}(z) = -\tan(\varphi_0)z$ (Figure 1(b)), we can obtain from equations (2) and (3)

$$\tan(\varphi_0) - E^{\Psi} \alpha_x \frac{\Delta T_b - \Delta T_a}{\tilde{h}_2} = 0 \quad (4)$$

The system of equations (1) and (4) represents the conditions of the problem which have to be satisfied. Since we have five unknowns (ΔT_a, ΔT_b, E^{Ψ}, α_x and α_z) and three equations, two parameters can be chosen arbitrarily, whereas the remaining three follow from the presented equations. Note that, in general, it cannot be evident which variables are (or could be) dependent on each other. In this particular case, however, that not all combinations of parameters are possible, for example, from equation (1), we can see that α_x and α_z together cannot be chosen arbitrarily.

The purpose of the section was to determine such properties and loadings of the TM beam Ψ_0^C, with which the $\Omega_{1\lambda}^C$ configuration of the idealised beam can be obtained directly from its stress-free Ω_2^C configuration.

TM model of the real beam and the stresses in the real beam, sub-steps 3.2 and 3.3. So far, we have shown that the idealised beam configuration $\Omega_{1\lambda}$ and its stresses can be calculated using two equivalent approaches: bending and the TMA approach. The idealised beam was first used to determine the properties of the idealised TM beam.

The activities performed in sub-step 3.1 now enable us to construct a new TM model Ψ_0 (Figure 3(b)) by
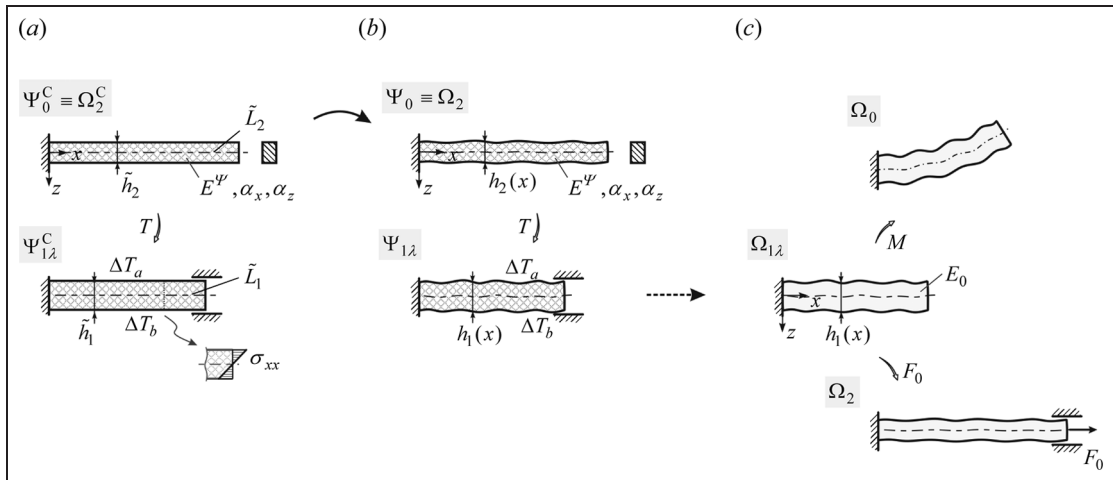
Figure 3. The TMA approach: (a) TM model of the idealised beam, (b) TM model of the real beam and (c) mechanical response of the original real beam (Figure 1(a)).

considering the geometry of the real beam Ω_2 (Figure 1(a)). Thus, the material data and the thermal loading are taken from the idealised TM beam model (section 'Determining the properties of the TM beam model, sub-step 3.1') and applied to the stress-free Ω_2 configuration (sub-step 3.2). In this way, we succeeded in obtaining a fair approximation of the $\Omega_{1\lambda}$ geometry and its respective residual stresses (Figure 3(b)). Finally (sub-step 3.3), to calculate any other configuration of the real beam in Figure 1(a), the material properties and loadings of the TM model $\Psi_{1\lambda}$ have to be switched to real material properties and loadings (Figure 3(c)).

To summarise, we have managed to obtain the residual stresses and the respective configuration of the real beam based on its loaded state configuration Ω_2. As will be shown later, this is especially welcome in the case of patient-specific arterial geometries since, first, only the in vivo arterial geometry is given and, second, the residual stresses and the corresponding configurations of an artery are obtained simply by applying the proper TMA properties directly to its stress-free in vivo geometry.

Applying the TMA approach to predict the mechanical response of an arterial segment

The purpose of this section is to present how the mechanical response of a real arterial segment can be predicted using the TMA approach. For the sake of brevity, we will treat the arterial segment as single-layered, isotropic and hyperelastic. In addition, the material properties of the segment are assumed to be known.

Let us observe the arterial segment in Figure 4(a) in its loaded state Ω_2. The goal is to predict the stresses in the observed state Ω_2, while the zero-stress configuration of the segment Ω_0 is unknown. In the loaded (in vivo) state Ω_2, the artery is loaded with blood pressure p. By removing the pressure, the segment shrinks in the radial direction and takes the so-called stretched state $\Omega_{1\lambda}$. By further cutting the segment transversely, the segment shrinks in the axial direction (for the stretch λ) and takes an unloaded state Ω_1. In this state, the artery is free of external loads but subject to internal (residual) stresses. By cutting the segment longitudinally, it springs open and takes the zero-stress state Ω_0.

This problem is treated, first, by simplifying (idealising) the geometry of the arterial segment (Figure 4(b)), performed, for instance, on area equivalence principle. For such an arterial segment, as will be shown, stresses for all of the configurations in Figure 4(b) can be determined. Next (step 3), the TMA approach is used to map the stresses of the idealised arterial segment (Figure 4(b)) onto the patient-specific arterial geometry (Figure 4(a)). Let us emphasise again that the properties of the TM model (i.e. its material behaviour and loadings) have no relation with the properties of the artery. As will be presented and clarified in the following, the behaviour of the artery is non-linear (and
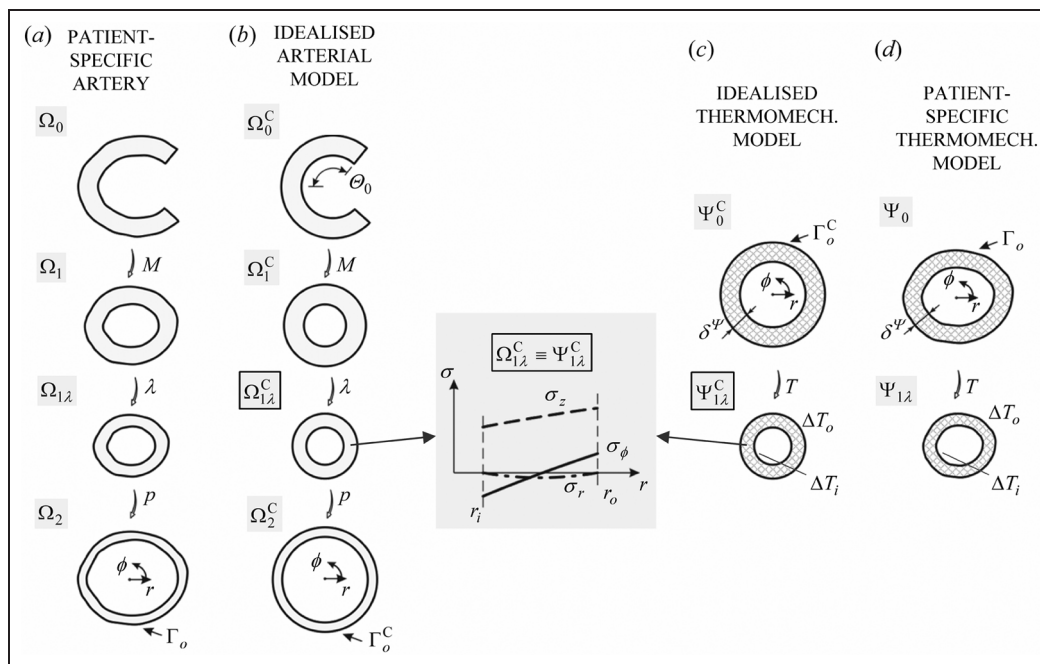
Figure 4. Predicting the mechanical response of a patient-specific arterial segment Ω_2: (a) patient-specific arterial segment, (b) idealised arterial segment, (c) idealised TM arterial segment and (d) TM model of patient-specific arterial segment.

undergoing large deformations), whereas the behaviour of the TM model is linearised.

In the following, the same steps will be followed as presented in the beam example. Therefore, to avoid presenting the TMA approach again in detail, parallels between the problems will be drawn throughout this section.

The initial (input) data of the problem, step 1. Similar to the beam example, the data that can be obtained when treating a patient-specific artery are the loaded (in vivo) configuration of the artery Ω_2 and the corresponding value of blood pressure p (Figure 4(a)). The material properties of the artery can be presumed from the literature or identified from the measured pressure dilatation waveform through the heart cycle of an artery.[15]

However, because we do not know the initial cut-open geometry of the arterial segment (Figure 4(a)), the stresses in its in vivo state cannot be computed. To estimate the mechanical response of the arterial segment, its shape is idealised into a circular one.

Idealised (circular) arterial segment, step 2. In this case, we know that the initial zero-stress state geometry Ω_0^C of the segment corresponds to a circular sector, where the value of the opening angle Θ_0 is unknown.

The key datum is the consideration of the uniform strain hypothesis.[7] Because the in vivo geometry Ω_2^C and the associated blood pressure of the idealised arterial segment are known, it is possible to determine and compute the response of all of the configurations of the idealised segment in Figure 4(b).[15]

Furthermore, with the mechanical response of the idealised arterial segment being known, the TMA approach is performed in order to transfer the idealised configuration $\Omega_{1\lambda}^C$ to the configuration $\Omega_{1\lambda}$ of the original (patient-specific) arterial segment.

TM model of the idealised arterial segment, sub-step 3.1. The purpose of this section is to obtain the residual stresses in the idealised arterial segment using an alternative approach, the idealised TM model Ψ_0^C (Figure 4(c)). The targeting state that we want to predict using the TMA approach is the stretched state $\Omega_{1\lambda}^C$ in Figure 4(b). The geometry of the initial zero-stress state of the TM arterial model Ψ_0^C follows from the in vivo geometry of the idealised artery Ω_2^C: the outer surface of the arterial segment Γ_0^C represents the outer surface of the TM model Ψ_0^C, whereas its thickness δ^Ψ needs to be properly determined.

The remaining properties of the TM model that need to be properly determined are the temperature loadings ΔT_o and ΔT_i, which need to be applied to the outer and inner surfaces, and the material properties, which need

to be different in the transverse ($r - \varphi$) and longitudinal (z) directions of the segment. This is required in order for the TM model to match the targeting configuration and the corresponding stresses.

The cross-sectional temperature distribution of the TM model is obtained by solving a steady-state heat exchange problem. During thermal loading, the TM segment is fixed in the axial direction (z) in order to obtain the proper value of axial stresses σ_z and to preserve the segment's axial dimension. Additionally, because the residual stresses in $\Omega_{1\lambda}^C$ are small in comparison to the stresses in the arterial loaded (in vivo) state, the material behaviour of the TM model is linearised. The material behaviour of the TM model is thus assumed to be linearly elastic and transversely isotropic with respect to the segment's z-direction.

Approximation of the original (patient-specific) arterial segment's stretched state $\Omega_{1\lambda}$, sub-step 3.2. Finally, the material properties and thermal loadings of the idealised TM segment are transferred to the stress-free geometry of the patient-specific in vivo geometry Ω_2 (Figure 4(c)). The obtained stresses and geometry in configuration $\Psi_{1\lambda}$ represent an approximation of the residual stresses and the corresponding configuration of the patient-specific arterial segment $\Omega_{1\lambda}$.

Furthermore, to obtain the state of the artery $\Omega_{1\lambda}$ – that is, to obtain a numerical model of the arterial residual stress state that can further be used to compute the arterial response presented in Figure 4(a) – the material properties and loadings of the TM model $\Psi_{1\lambda}$ have to be switched to the material properties and loadings of the arterial segment (sub-step 3.3). It is worth emphasising again that in sub-step 3.3, a completely new (arterial) model is defined whose material behaviour (and loading) is in no relation with the (linear) material behaviour (or loading) of the TM model.

Summary of the TMA approach

For clarity, let us once again summarise the key steps of the TMA approach in the case of treating an arterial segment (Figure 5):

1. From the experimental data of a patient-specific arterial segment (Figure 4(a)), that is the in vivo configuration Ω_2 and the corresponding blood pressure p, the idealised arterial segment is defined.
2. By adopting the uniform strain hypothesis, all of the configurations for the circular arterial segment can be computed (Figure 4(b)).
3. Based on the obtained stress state and configuration $\Omega_{1\lambda}^C$ of the circular arterial segment, the
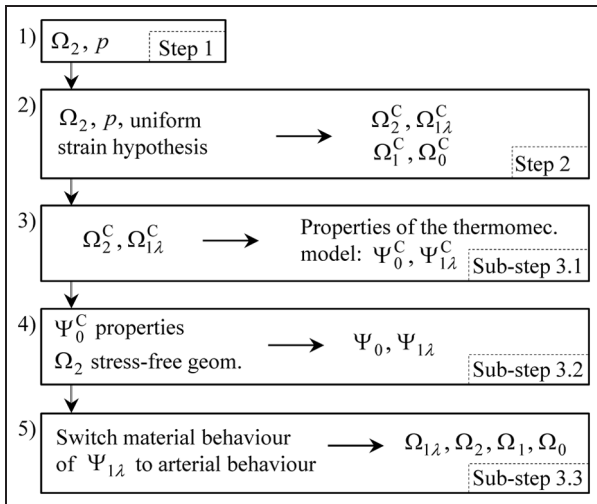
Figure 5. Steps of the TMA approach for treating a patient-specific arterial segment.

corresponding circular TM model Ψ_0^C is defined (Figure 4(c)).

4. The TM model of the patient-specific arterial segment Ψ_0 is obtained next by applying properties of Ψ_0^C to the stress-free in vivo patient-specific arterial geometry Ω_2 (Figure 4(d)).

5. By switching the material properties and loadings of $\Psi_{1\lambda}$ to the arterial ones, all of the configurations of the original (patient-specific) arterial segment in Figure 4(a) are obtained.

Experimental data

CCA was examined in a healthy 28-year-old and non-smoking male. Prior to taking measurements, the subject was asked to rest for 15 min.

CCA geometry

The CCA in vivo configuration was obtained through the use of a high-resolution echo-tracking device,

Philips iU22 (Philips Healthcare), and a L9-3 linear probe by an experienced cardiovascular surgeon. While recording the ultrasound (US) signals of the CCA transversal view, the US probe was moved from approximately 60 mm proximal to the carotid bulb to 30 mm distal to the bulb. The time of the recording was approximately 2 min, and the speed of the probe was kept nearly constant. In order to obtain the spatial position of the probe, its longitudinal movement was recorded with a camera. Throughout the measurement, the subject was monitored via electrocardiogram (ECG).

Segmentation of the artery. The US recording was first segmented into time frames. Based on the ECG data, the frames that corresponded to the CCA systolic state were selected, and points on the outer (media) wall contour of the CCA were manually picked. Since the shape of the arterial cross section is roughly elliptic,[16] we designed an algorithm that placed a best-fitting ellipse to the selected points. The longitudinal positions of the ellipses along the CCA were obtained by synchronising the US recording of the arterial transversal view and the recording of the US probe with time. Finally, by interpolating a surface through the positioned ellipses, the outer (*o*) systolic state (*s*) surface of the analysed CCA was obtained and designated as Γ_o^s (Figure 6(a)). The section of the CCA that is observed in this work is shown in Figure 6(b).

CCA pressure–radii waveform

For the characterisation of a circular arterial segment based on the in vivo measured data, pressure distention data of a CCA section are needed. However, in contrast to section 'Applying the TMA approach to predict the mechanical response of an arterial segment', when a single arterial cross section was observed, the cross section of the CCA is variable. In this case, therefore, at least two sections along the CCA need to be observed, which are designated as sections (m) and (M). Their location along the CCA is shown in Figure 7(a), where the
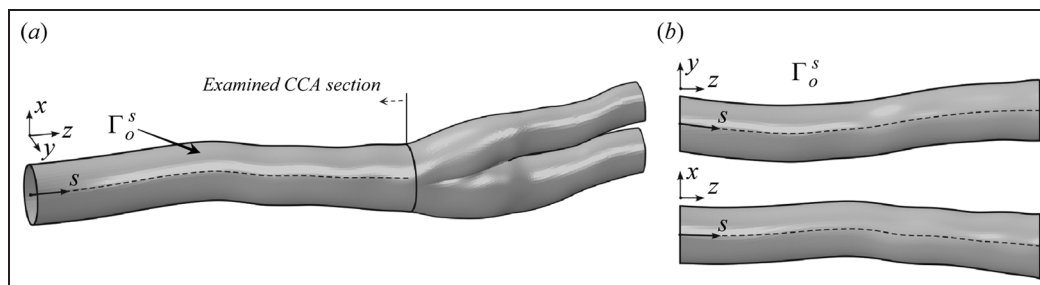
Figure 6. The reconstructed outer systolic surface of the CCA Γ_o^s.
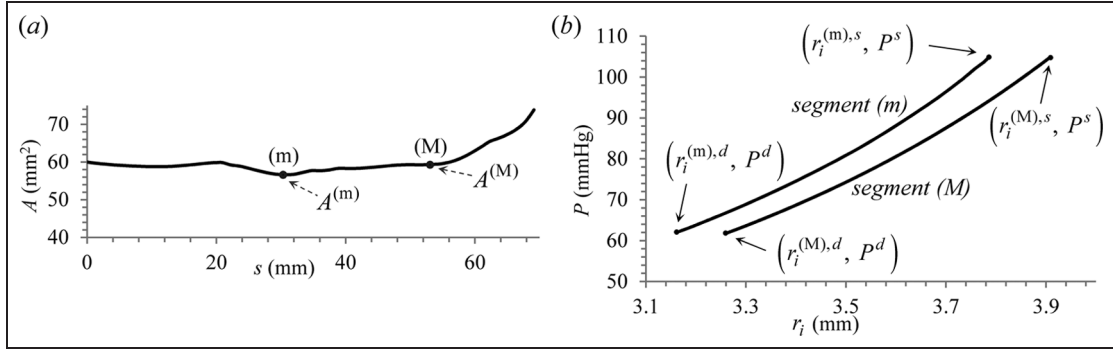
Figure 7. Variation of the cross-sectional area of the surface Γ_o^s (designated as $A(s)$) along the CCA centreline s and (b) the pressure–radius cycle at CCA locations (M) and (m), where P^s and P^d represent the systolic and diastolic value of blood pressure $P(t)$, respectively.

variation of the CCA cross-sectional area $A(s)$ along the centreline coordinate s is presented. In the following, the aim is to obtain the pressure distension waveform for both observed sections – (m) and (M) – along the CCA.

The CCA distension waveform $r_i^{(M)}(t)$ was obtained using M-mode imaging, which was measured at location (M) along the CCA (Figure 7(a)). Additionally, from the M-mode images, an average intima-media thickness (IMT) in the CCA systolic state δ_s was obtained, being $\delta_s = 0.45$ mm. In this work, the IMT in the CCA systolic state was assumed to be constant along the entire CCA section, being δ_s.

The CCA pressure waveform $P(t)$ was obtained from the CCA radius waveform $r_i^{(M)}(t)$ by combining the diameter-derived pulse pressure method[17] and the exponential relationship between the arterial cross-sectional area and the pressure[18,19] (Appendix 1). The pressure–radii waveform $P - r_i^{(M)}$ was obtained by combining $P(t)$ and $r_i^{(M)}(t)$, as presented in Figure 7(b).

Modelling the CCA mechanical response

Mechanical behaviour of the CCA

In this section, the TMA approach is applied to the observed CCA with the purpose of predicting its residual stress state. As already mentioned, in contrast to characterising a single arterial section, as was presented in section 'Applying the TMA approach to predict the mechanical response of an arterial segment', the cross section of the CCA is variable. This means that, in general, any number of CCA sections could be observed to define their corresponding TM segments. In this work, for the sake of brevity, two locations along the CCA are observed: locations (m) and (M), as shown in Figure 7(a).

The CCA is modelled as hyperelastic, isotropic and incompressible. For the material behaviour, the following strain energy density function is assumed[2]

$$W = \frac{c_a}{c_b}\left[\exp\left[\frac{c_b}{2}(I_1 - 3)\right] - 1\right] \tag{5}$$

where I_1 is the first invariant of the right Cauchy–Green tensor $\mathbf{C}$, given as $\mathbf{C} = \mathbf{F}^{\mathrm{T}}\mathbf{F}$ (where $\mathbf{F}$ is the deformation gradient tensor), and c_a and c_b are constitutive model parameters referring to the observed CCA. In this work, the artery is treated as single layered, taking into account the intima-media layer. The effect of adventitia can be considered as a pressure load, applied on the outer side of the artery.[20,21] Since this is performed in the step of characterising a circular arterial segment, this does not influence the mapping of stresses from the circular to the actual arterial geometry, which means it does not limit the use of the TMA approach.

In this work, we will determine the values of CCA material parameters based on the in vivo data obtained. The feasibility of characterising the arterial material properties based on the in vivo clinical data was demonstrated by Masson et al.,[20] Schulze-Bauer and Holzapfel[22] and Stålhand et al.[23] This is performed by treating an idealised (circular) arterial segment. In addition to obtaining the geometry of the segment's initial configuration, the material parameters are identified as well.

Using the TMA approach, the CCA residual stress state is predicted by applying the properties of the circular TM CCA segment to the in vivo measured CCA geometry, as presented in section 'Applying the TMA approach to predict the mechanical response of an arterial segment'. First, a circular segment of the CCA needs to be fully characterised. Then, the TMA approach is applied to 'transfer' the residual stresses and configuration(s) from a circular CCA segment to a patient-specific CCA geometry. Because the cross-sectional area of the CCA changes, two sections along the CCA need to be observed. For these two segments, by idealising their geometry, the material properties and the zero-stress state geometry are determined. To 'transfer' their mechanical response to the patient-

specific CCA, two circular TM segments are then defined, each corresponding to individual circular CCA segment. Finally, to obtain an approximation of the CCA residual stress state, the properties of both TM segments (i.e. their loadings and material properties) are interpolated/extrapolated along the CCA and applied to the CCA stress-free in vivo geometry Γ_o^s. In the following sub-sections, the individual steps of the approach are presented in detail.

Circular CCA segments

The purpose of this section is to characterise the two circular CCA segments. The segments correspond to positions (M) and (m) along the CCA. Luminal (inner) diameter of segments is obtained from the luminal cross-sectional area of the CCA (measured at its corresponding locations, Figure 7(a)). Segments are treated with the purpose, on one hand, of obtaining the material properties of the CCA and, on the other hand, of obtaining the referential residual stress state(s), based on which the TM model will then be calibrated.

First, the segment (M) is treated, and its initial geometry and CCA material properties are identified. Afterwards, by adopting the obtained material properties, the segment (m) is characterised in order to determine its initial zero-stress geometry.

The parameters that need to be determined for the circular arterial segment (M) are the zero-stress state radius $R_o^{(M)}$, the opening angle $\Theta_o^{(M)}$ (see Figure 4(a)) and the material parameters c_a and c_b, equation (5). These are obtained by solving a minimisation problem using the in vivo pressure distention data, as presented by Stålhand.[15] The classical mathematical framework for treating a circular arterial segment and the details of the identification procedure are given in Appendix 2. The obtained values of the identified parameters are tabulated in Table 1.

After adopting the obtained material parameters, the segment (m) is treated next in order to identify its zero-stress state radius $R_o^{(m)}$ and opening angle $\Theta_0^{(m)}$. The identification procedure is similar to that performed for the segment (M) (Appendix 2). The values of the identified parameters are given in Table 1.

Table 1. The identified properties of the circular arterial segments (M) and (m).

Segment: k	(M)	(m)
$R_0^{(k)}$ (mm)	5.14	5.48
$\Theta_0^{(k)}$ (°)	115.56	105.24
Material properties	$c_a = 72.1$ kPa	
	$c_b = 1.14$	

Circular TM segments

With circular CCA segments (M) and (m) completely defined, the properties and loadings of their corresponding TM segments, (M) and (m), can be determined next. First, the segment (M) is treated. Its initial geometry is defined based on the in vivo (systolic) stress-free geometry of the CCA segment (M), whereas its properties are determined in such a way that its loaded state matches the CCA segment's stretched state $\Omega_{1\lambda}^C$ stresses and geometry. Next, in a similar fashion, the circular TM segment (m) is treated. In doing so, some of the properties obtained for the TM segment (M) are already adopted, as will be presented in the following.

The properties of TM segments that are common for both segments are E_P^Ψ, E_T^Ψ and α_P, being the elastic moduli in the 'in-plane' (P) and transverse (T) directions and the coefficient of thermal expansion in P direction, whereas the properties that relate to individual segment are $\delta^{\Psi(k)}$, $\alpha_T^{(k)}$ and $\Delta T_i^{(k)}$, $\Delta T_o^{(k)}$; $k \in \{m, M\}$, being the thicknesses of each segment, the coefficient of thermal expansion in T direction, and thermal loadings.

In computing the mechanical response of the TM model, we can treat the problem as a sequentially coupled steady-state thermal-stress problem. This means that, first, the steady-state heat conduction problem must be solved, where the temperature distribution over the thickness of the segment is obtained based on the applied thermal loadings. The obtained temperature field is then applied as the loading to the stress analysis in order to obtain the mechanical response of the TM model. The mathematical relations that are needed to compute the steady-state thermomechanical response of the circular TM segment are given in Appendix 3.

The values of the unknowns defining both circular TM segments are obtained by solving a minimisation problem, as shown in Appendix 3. The obtained best-fit values are presented in Table 2.

In the following, the obtained parameters of both TM segments are applied to the in vivo stress-free geometry of the CCA. However, since some parameters refer to each TM segment individually, their values first have to be properly interpolated/extrapolated in order to be applied to the CCA in vivo geometry.

Generalising the properties of the TM segments

In order to apply the properties of the circular TM segment to the in vivo CCA geometry, the properties that refer to the individual TM segment (ΔT_o, ΔT_i, δ^Ψ and α_T) need to be interpolated/extrapolated (or generalised) along the CCA cross-sectional area $A(s)$. Since two TM segments were observed, a linear interpolation between both cross-sectional areas is applied.

Table 2. The identified properties of the TM circular segments.

Segment: k	M	m
$\Delta T_i^{(k)}$ (°C)	0.949	0.895
$\Delta T_o^{(k)}$ (°C)	1.283	1.288
$\delta^{\Psi(k)}$ (mm)	0.847	0.836
$\alpha_T^{(k)}$ (1/K)	−0.0394	−0.040
E_P^{Ψ} (kPa)	273.15	
E_T^{Ψ} (kPa)	505.04	
α_P (1/K)	−0.216	

TM: thermomechanical.
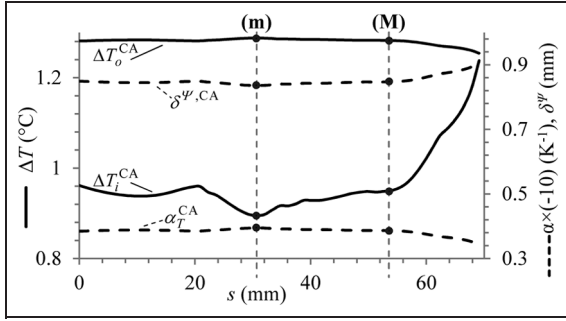
Figure 8. Variations of the fictitious CCA model properties: $\alpha_T^{CA}(s)$, $\delta^{\Psi, CA}(s)$, $\Delta T_i^{CA}(s)$ and $\Delta T_o^{CA}(s)$ along the coordinate s.

A linear interpolation of a variable, say, α_T^{CA} (where the superscript 'CA' refers to the interpolated variable), ranging from $A^{(M)}$ to $A^{(m)}$, is written as follows

$$\alpha_T^{CA}(A(s)) = \alpha_T^{(m)}\left(1 - \frac{A(s) - A^{(m)}}{A^{(M)} - A^{(m)}}\right)$$
$$+ \alpha_T^{(M)}\left(\frac{A(s) - A^{(m)}}{A^{(M)} - A^{(m)}}\right) = \alpha_T^{CA}(s) \quad (6)$$

where $\alpha_T^{(m)} = \alpha_T(A^{(m)})$ and $\alpha_T^{(M)} = \alpha_T(A^{(M)})$. The same interpolation approach is used to define the remaining variables: $\delta^{\Psi, CA}(s)$, $\Delta T_i^{CA}(s)$ and $\Delta T_o^{CA}(s)$. Their variations as a function of the coordinate s are plotted in Figure 8.

The parameters that are assumed the same for both TM segments (m) and (M) are also assumed to be constant along the CCA.

TM model of the CCA

To obtain the approximation of the CCA residual stress state (i.e. stresses and geometry), we apply the parameters and loadings that were obtained for the circular TM segments to the in vivo CCA stress-free geometry Γ_o^s. In this way, essentially, the TM model of the real CCA is obtained. The initial (zero-stress) configuration of the model Ψ_0 is presented in Figure 9.

Note that the thickness of the model Ψ_0 is assumed to be constant in its circumferential direction, whereas it changes in the s direction, according to Figure 8. For the computation of the TM response of the TM model, the finite element (FE) method is used. The model was discretised into cca. 67,200 eight-node hexaedral FE elements (Figure 9). While applying the temperature changes $\Delta T_i^{CA}(s)$ and $\Delta T_o^{CA}(s)$, the model's front and rear surface are kept axially fixed. Note that both $\Delta T_i^{CA}(s)$ and $\Delta T_o^{CA}(s)$ are assumed to be constant in the circumferential direction of the model with respect to the s coordinate.

Results and discussion

Numerical computations of the TMA and the arterial CCA model were performed with ABAQUS/Standard. In the following, the predicted CCA stretched state $\Omega_{1\lambda}$ is presented first and discussed. Afterwards, in order to
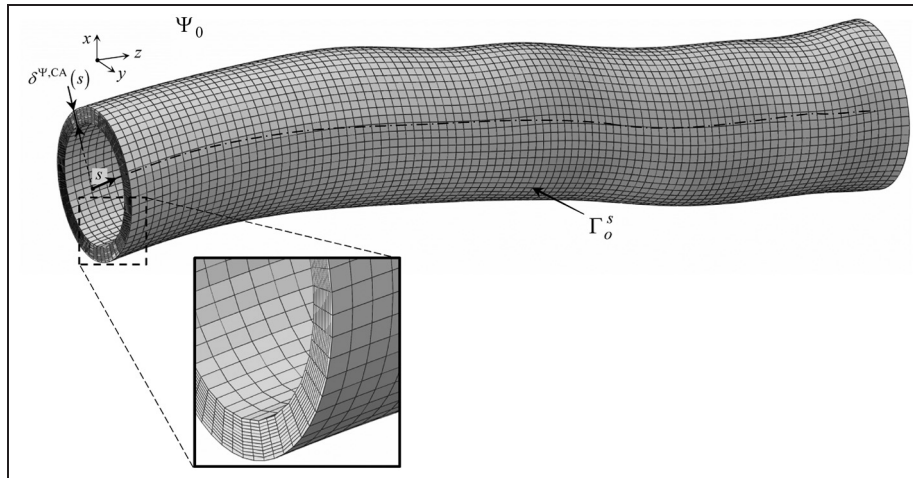
Figure 9. Finite element model of the TMA CCA model Ψ_0.
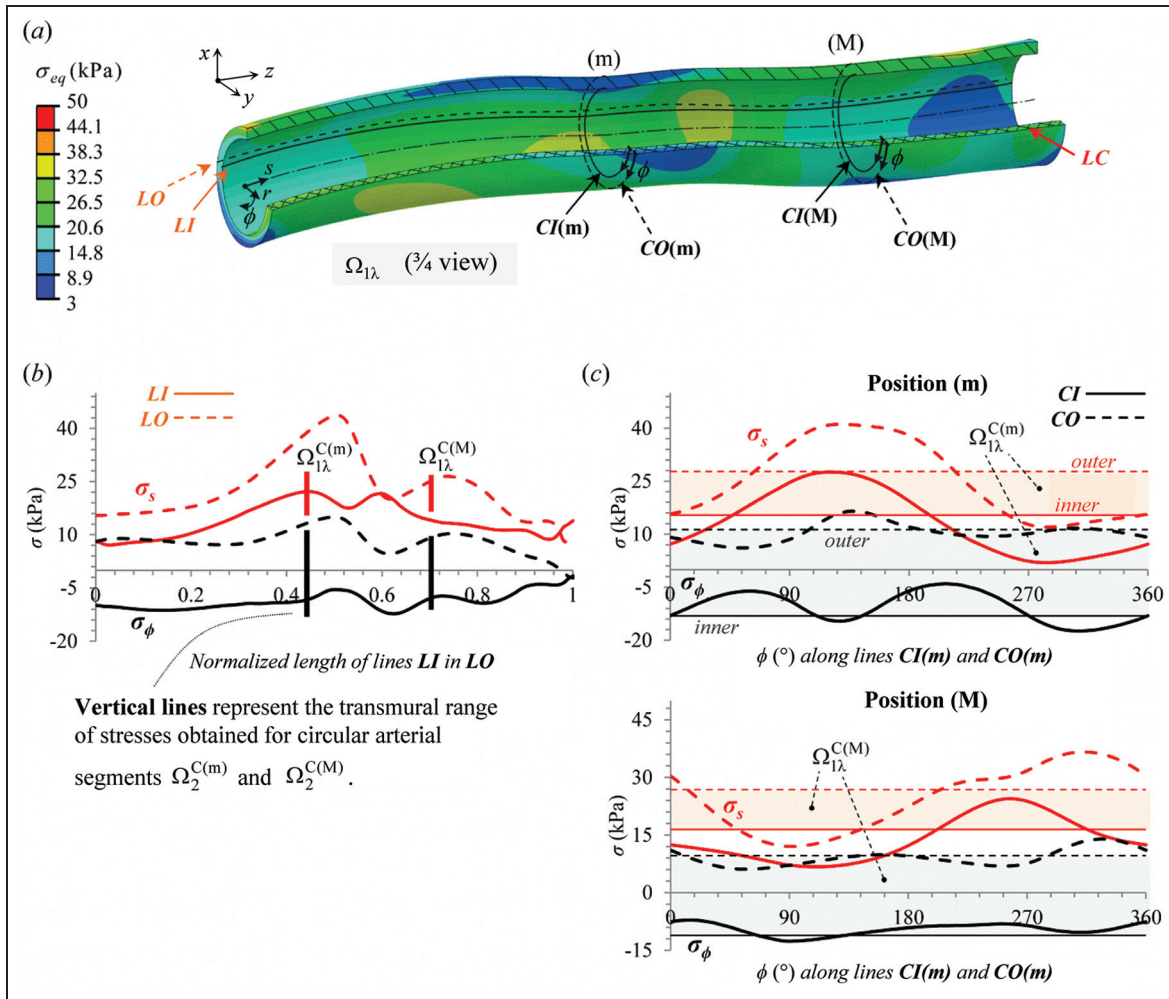
Figure 10. The predicted CCA stretched state ($\Omega_{1\lambda}$): (a) the von Mises equivalent stress, (b) the variation of stresses along lines *LI* and *LO* and (c) the variation of stresses along lines *CI* and *CO* at locations (m) and (M). Figures (b) and (c) also show the stresses predicted for circular arterial segments (M) and (m): $\Omega_{1\lambda}^{C(M)}$ and $\Omega_{1\lambda}^{C(m)}$.

validate partially the methodology, the prediction of the CCA systolic state is presented where we compare the predicted CCA geometry to the measured one. Finally, the predicted zero-stress state Ω_0 is given.

Stretched state of the CCA

The predicted CCA stretched state $\Omega_{1\lambda}$ is presented in Figure 10(a). As shown in the figure, the stresses vary significantly over the entire CCA, which is the consequence of the CCA's irregular geometry. The same can be observed in Figure 10(b), where the variations of the longitudinal σ_s and circumferential σ_ϕ stresses along the lines *LI* and *LO* (located on the internal and external surface of the CCA, Figure 10(a)) are presented. Because the CCA stretched state is also axially prestretched, σ_s is the dominant stress. By observing the σ_ϕ stress along *LI* and *LO*, their bending-like distribution is seen. σ_ϕ is compressive at the inner CCA surface

(line *LI*, full curve) with an average value of cca. $-8\,kPa$ and tensile at the outer surface (line *LO*, broken curve) with an average value of cca. $10\,kPa$. In comparison with the existing data from the literature, in Alastrué et al.,[24] the bending residual stresses were predicted for a human iliac artery, ranging from cca. -12 to $11.6\,kPa$. In Alastrué et al.,[6] a slice of human coronary artery was observed, and the predicted residual stresses ranged from cca. -8 to $6.5\,kPa$. Although different arteries were treated in Alastrué et al.[6,24] than in our work, the range of the predicted (bending) residual stresses is in agreement. Furthermore, in Delfino,[25] a section of a CCA is treated with the same material constitutive model as that which is used in this work. Thereby, the predicted bending residual stresses range from cca. -6 to $6\,kPa$, which also agrees well with the data obtained in our work.

The comparison of our results with the data from the literature serves as a quantitative validation of the
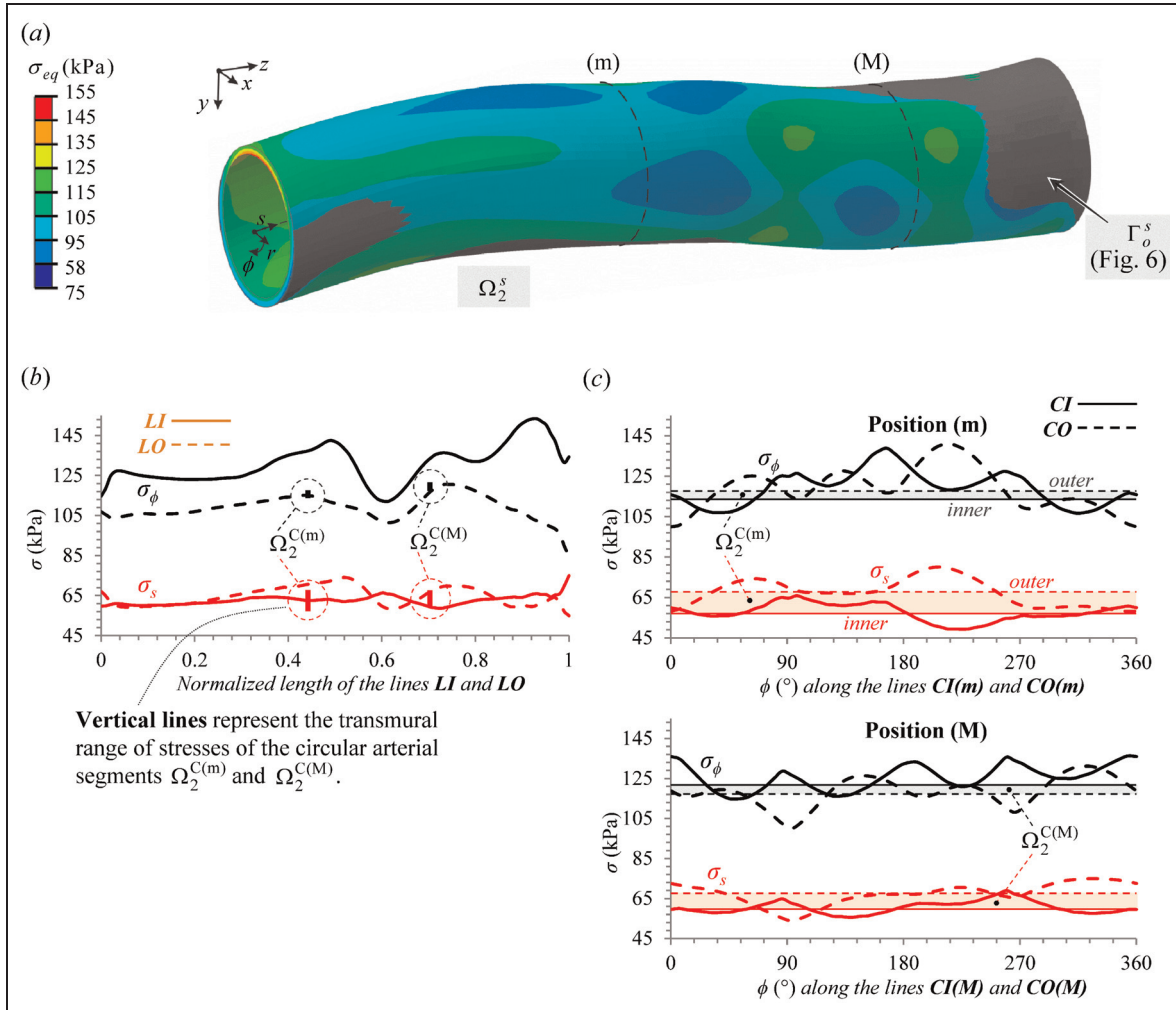
Figure 11. The predicted CCA systolic state (Ω_2^s): (a) the von Mises equivalent stress, (b) the variation of stresses along lines *LI* and *LO* and (c) the variation of stresses along lines *CI* and *CO* at location (m) and (M). Figures (b) and (c) also show the stresses predicted for circular arterial segments (M) and (m): $\Omega_2^{C(M)}$ and $\Omega_2^{C(m)}$. The measured (referential) CCA surface Γ_o^s in Figure (a) is shown in grey.

approach. We need to emphasise that the validation of the predicted residual stress of the CCA could be performed only experimentally, which is beyond the scope of this work.

Furthermore, let us compare the stresses predicted for the CCA stretched state with the stresses predicted by the circular arterial segments (M) and (m), designated as $\Omega_{1\lambda}^{C(M)}$ and $\Omega_{1\lambda}^{C(m)}$, respectively. The transmural range of $\Omega_{1\lambda}^{C(M)}$ and $\Omega_{1\lambda}^{C(m)}$ stresses is presented in Figure 10(b) with vertical lines, whereas the position of the lines corresponds to the location of the (m) and (M) segments. The range of σ_s stresses somewhat differs between the circular segments and the CCA model, whereas the range of circumferential stresses σ_ϕ does not deviate significantly.

The variations of CCA stresses along lines *CI* and *CO* are presented in Figure 10(c). The variation of stresses, as seen in the figure, obtains a periodic sine-like

distribution with large variation in magnitude. This can be attributed to the variable longitudinal curvature (radius and the curvature centre) of the CCA. For comparison, the stresses that are predicted for the circular arterial segments $\Omega_{1\lambda}^{C(M)}$ and $\Omega_{1\lambda}^{C(m)}$ are also presented in the figure (straight lines). As can be seen, a large deviation between stress distributions was obtained for the CCA and circular segments.

Loaded state of the CCA

The predicted CCA systolic state (Ω_2^s) is shown in Figure 11(a), whereas the variation of stresses σ_ϕ and σ_s along lines *LI* and *LO* (Figure 10(a)) is shown in Figure 11(b). As seen in the figure, the stresses vary considerably along the entire CCA as was also observed for the CCA stretched state. Note, however, that the slight increase in σ_s, which occurs at the end of the lines
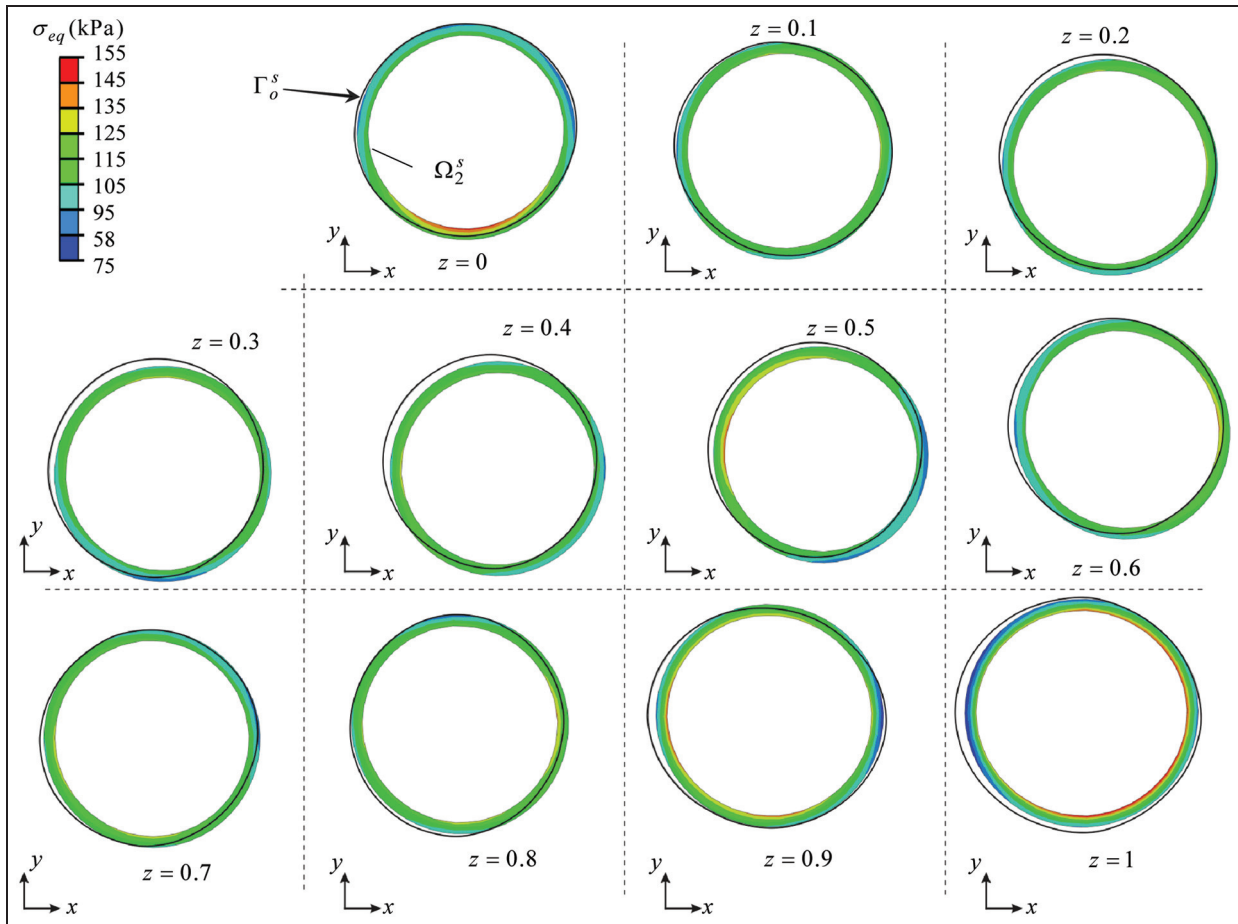
Figure 12. Individual cross sections of the model presented in Figure 11(a), obtained by dividing the model in Figure 11(a) into 10 equidistant parts along the coordinate z – note that the cross sections of the surface Γ_o^s are shown in black. z is the normalised coordinate: z = [0,1].

LI and *LO*, is a consequence of the boundary conditions. As a result of the applied pressurised load, the dominant stress in Ω_2^s is the circumferential stress σ_ϕ. The magnitude of the predicted stresses is in quantitative agreement with the corresponding data available from the literature.[2,26]

Moreover, the transmural range of $\Omega_2^{C(m)}$ and $\Omega_2^{C(M)}$ stresses is presented in Figure 11(b) with vertical lines, whereas the position of the lines corresponds to the location of the (m) and (M) segments. The stresses at the inner surface of the artery, predicted with the circular arterial segments, are for more than 15% underestimated in comparison to the corresponding stresses, predicted for the CCA (Ω_2^s). The inhomogeneous distribution of the CCA stresses, which cannot be predicted if we observe a circular CCA segment alone, is a consequence of geometrical irregularities of the CCA. However, if we take into consideration the uniform strain hypothesis, which, in a way states that the transmural distribution of stresses in the arterial state in vivo tends to be homogeneous, the physical objectivity

of the results presented is somewhat questionable, which indicates the need to further analyse and develop the presented methodology.

The variation of the CCA stresses along lines *CI* and *CO* (Figure 10(a)) is presented in Figure 11(c). For comparison, the corresponding stresses predicted for the circular arterial segments (m) and (M) are presented in the figure with straight lines. As observed in the previous section, the stresses of the CCA Ω_2^s state vary strongly in the circumferential direction and differ considerably from the corresponding stresses predicted for the circular segments. The predicted distribution of the CCA stresses exhibits a periodic sine-like distribution, as observed in the stretched state of the CCA which can be attributed to the CCA longitudinal curvature. However, considering the tendency of the CCA stress state to be nearly homogeneous, it is unlikely that such a severe stress gradient would appear in the CCA circumferential direction. We could speculate that in order to obtain more homogeneous stresses along the CCA, the arterial longitudinal curvature as well as its
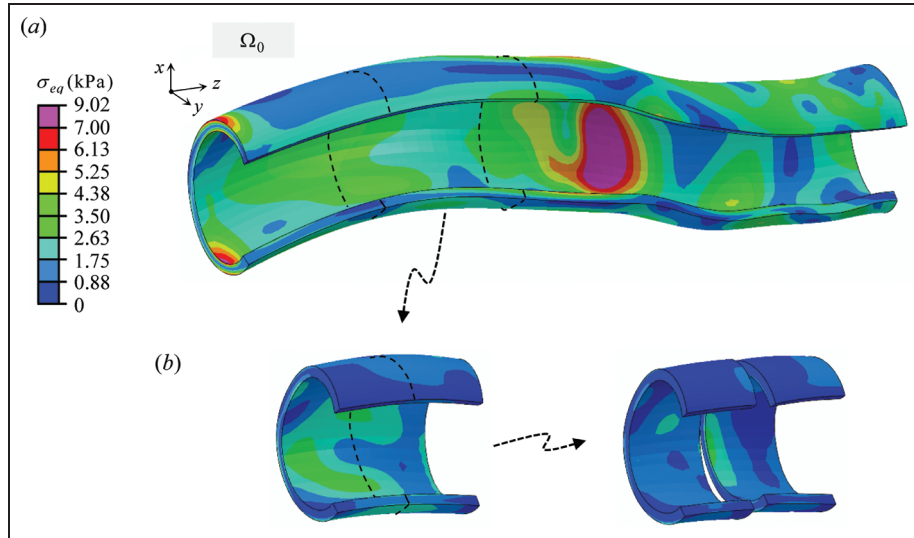
Figure 13. Predictions of the CCA zero-stress state: (a) the cut-open state of the CCA Ω_0 and (b) the release of residual stresses when the CCA is further split into smaller pieces.

variable cross section would have to be taken into consideration in the earlier stages of the CCA characterisation, that is, when predicting the mechanical response of the circular arterial segment.

In Figure 11(a), the comparison between the predicted CCA configuration and the measured CCA surface in vivo Γ_o^s (shown in grey) is presented. However, for a better comparison between both configurations, individual cross-sectional views of Figure 11(a), which we obtain by dividing the CCA in Figure 11(a) into 10 equidistant sections along the coordinate z, are presented in Figure 12. It is seen in the figure that the deviation between both configurations is somewhat bigger at $z = (0.3–0.6)$ which corresponds to the regions where the CCA is somewhat more longitudinally curved. This deviation is a result of the longitudinal stretching of the CCA (which in our case occurs in the TM model of the CCA during the thermal loading) which has an effect of straightening the CCA. Moreover, the predicted CCA cross-sectional areas are slightly more round in comparison to the measured configuration. This is seen at $z = (0.8, 0.9)$ and is a result of the inflation of the CCA model by blood pressure. The agreement between the configurations could, for instance, be somewhat improved, if we took into consideration the surrounding tissue. Nevertheless, the overall agreement between both configurations is satisfactory.

Zero-stress state of the CCA

The appropriateness of the TMA approach for predicting the CCA residual stress state can be validated by predicting the CCA zero-stress state configuration Ω_0.

Because the residual stresses exhibit a bending-like distribution, a cut-open configuration is expected for the CCA zero-stress state.

An approximation of the CCA zero-stress state Ω_0 is presented in Figure 12(a). Ω_0 is obtained by computing the equilibrium response of the CCA after the axial stretch λ is released from $\Omega_{1\lambda}$, followed by a longitudinal cut over the *LC* surface (shown in Figure 10(a)). It can be seen in the figure that the CCA obtained a sector-like shape, which indicates the existence of bending-like stresses in the CCA stretched state $\Omega_{1\lambda}$.

The peak value of the von Mises equivalent stress in Ω_0 is around 9 kPa and occurs locally in the middle area of the CCA. The reason why some of the residual stress still exists in Ω_0 is because of the CCA's variable cross-sectional area. Namely, in order to obtain a complete stress-free configuration, the CCA should be split further into an infinite number of material points.[8] This is seen in Figure 13(b), where the portion of the CCA is split further. As the results show, the more the CCA is cut into smaller pieces, the more its residual stresses are relieved (Figure 13).

Conclusion

Many soft biological tissues show volumetric growth which results in the development of residual stresses in their load-free configuration.[8,27,28] In this work, the residual stress state of a human CCA is predicted using the TMA approach. The approach is used in order to perform kinematically and statically consistent mapping of the residual stress state obtained for a circular arterial segment (i.e. its stresses and the corresponding configuration) onto the patient-specific arterial geometry.

CCA is examined on a healthy 28-year-old male using non-invasive methods, where an isotropic and hyperelastic material model was used to account for the CCA's mechanical behaviour. With TMA approach, the CCA's residual stress state is obtained by applying proper volumetric dilatations to the actual stress-free in vivo CCA geometry. The amount of the applied dilatation is obtained by observing two individual CCA sections and predicting their mechanical responses by idealising their geometry into a circular one. The predicted CCA residual stresses are in good quantitative agreement with the data of residual stresses in arteries found in the literature. Additionally, in order to validate the approach, first, the predicted CCA loaded state geometry was computed to the measured CCA geometry. The agreement between both data was found to be satisfactory. Second, the zero-stress state of the CCA is predicted. As known in the literature, a cut-open state is obtained with the residual stresses almost vanishing.

A limitation of this work is that the artery is treated in a rather simplified manner by adopting an isotropic material behaviour and a one-layer structure. However, since the TMA approach performs or affects only the mapping from a circular arterial segment to patient-specific arterial geometry, considering a multi-layered structure and an anisotropic material behaviour does not represent a limitation for the approach.

In applying the approach to an artery of a variable thickness, as occurs in the case of atherosclerotic arteries, the uniform strain hypothesis is questionable. Still the presented approach is applicable with a new assumption adopted that would have to be identified based on experimental data of atherosclerotic arteries.

The benefit of the approach is that it enables the use of medical image acquisition techniques (such as magnetic resonance imaging (MRI), computed tomography (CT) or US) to model the artery's residual stresses and its respective configuration. The inability to predict the arterial residual stress state configuration represents a major drawback of most of the existing methods in the literature. Although these methods predict the residual stresses, the prediction of the corresponding arterial geometry is not that trivial and iterative approaches need to be used, as for instance presented in Sellier.[29] Along with the non-invasive medical imaging techniques, we believe that the TMA approach could serve as a useful tool to develop a better understanding of the in vivo stress state of patient-specific arterial geometry.

Declaration of conflicting interests

The author(s) declared no potential conflicts of interest with respect to the research, authorship, and/or publication of this article.

References

1. Sommer G, Regitnig P, Költringer L, et al. Biaxial mechanical properties of intact and layer-dissected human carotid arteries at physiological and supraphysiological loadings. *Am J Physiol Heart Circ Physiol* 2010; 24: H898–H912.
2. Delfino A, Stergiopulos N, Moore JE Jr, et al. Residual strain effects on the stress field in a thick wall finite element model of the human carotid bifurcation. *J Biomech* 1997; 30: 777–786.
3. Holzapfel GA and Ogden RW. Modelling the layer-specific three-dimensional residual stresses in arteries, with an application to the human aorta. *J R Soc Interface* 2010; 7: 787–799.
4. Wang R and Gleason RL. A mechanical analysis of conduit arteries accounting for longitudinal residual strains. *Ann Biomed Eng* 2010; 38: 1377–1387.
5. Chuong CJ and Fung YC. On residual stresses in arteries. *J Biomech Eng* 1986; 108: 189–192.
6. Alastrué V, Pena E, Martinez MA, et al. Assessing the use of the 'opening angle method' to enforce residual stresses in patient-specific arteries. *Ann Biomed Eng* 2007; 35: 1821–1837.
7. Takamizawa K and Hayashi K. Strain energy density function and uniform strain hypothesis for arterial mechanics. *J Biomech* 1987; 20: 7–17.
8. Polzer B, Bursa J, Gasser CT, et al. A numerical implementation to predict residual strains from the homogeneous stress hypothesis with application to abdominal aortic aneurysms. *Ann Biomed Eng* 2013; 41: 1516–1527.
9. Zhou X and Lu J. Estimation of vascular open configuration using finite element inverse elastostatic method. *Eng Comput* 2009; 25: 49–59.
10. Schröder J and Brinkhues S. A novel scheme for the approximation of residual stresses in arterial walls. *Arch Appl Mech* 2014; 84: 881–898.
11. Skalak R, Zargaryan S, Jain RK, et al. Compatibility and the genesis of residual stress by volumetric growth. *J Math Biol* 1996; 34: 889–914.
12. Baek S, Rajagopal KR and Humphrey JD. A theoretical model of enlarging intracranial fusiform aneurysms. *J Biomech Eng* 2006; 128: 142–149.
13. Zeinali-Davarani S, Raguin LG and Baek S. An inverse optimization approach toward testing different hypotheses of vascular homeostasis using image-based models. *Int J Struct Chang Solid* 2011; 3: 33–45.
14. Urevc J, Flis V, Brumen M, et al. Applying thermomechanical analogy to predict the arterial residual stress state. *Strojniški vestnik – J Mech Eng* 2015; 61: 5–23.
15. Stålhand J. Determination of human arterial wall parameters from clinical data. *Biomech Model Mechanobiol* 2009; 8: 141–148.
16. Vukadinovic D, van Walsum T, Manniesing R, et al. Segmentation of the outer vessel wall of the common carotid artery in CTA. *IEEE Trans Med Imaging* 2010; 29: 65–76.

17. Van Bortel LM, Balkestein EJ, van der Heijden-Spek JJ, et al. Non-invasive assessment of local arterial pulse pressure: comparison of applanation tonometry and echo-tracking. *J Hypertens* 2001; 19: 1037–1044.

18. Meinders JM and Hoeks AP. Simultaneous assessment of diameter and pressure waveforms in the carotid artery. *Ultrasound Med Biol* 2004; 30: 147–154.

19. Vermeersch SJ, Rietzschel ER, De Buyzere ML, et al. Determining carotid artery pressure from scaled diameter waveforms: comparison and validation of calibration techniques in 2026 subjects. *Physiol Meas* 2008; 29: 1267–1280.

20. Masson I, Boutouyrie P, Laurent S, et al. Characterization of arterial wall mechanical behavior and stresses from human clinical data. *J Biomech* 2008; 41: 2618–2627.

21. Humphrey JD and Na S. Elastodynamics and arterial wall stress. *Ann Biomed Eng* 2002; 30: 509–523.

22. Schulze-Bauer CAJ and Holzapfel GA. Determination of constitutive equations for human arteries from clinical data. *J Biomech* 2003; 36: 165–169.

23. Stålhand J, Klarbing A and Karlsson M. Towards in vivo aorta material identification and stress estimation. *Biomech Model Mechanobiol* 2004; 2: 169–186.

24. Alastrué V, Martinez MA and Doblare M. Modelling adaptative volumetric finite growth in patient-specific residually stressed arteries. *J Biomech* 2008; 41: 1773–1781.

25. Delfino A. *Analysis of stress field in a model of the human carotid bifurcation*. Lausanne: Department of Physics, Ecole Polytechnique Federale de Lausanne, 1996.

26. Masson I, Beaussier H, Boutouyrie P, et al. Carotid artery mechanical properties and stresses quantified using in vivo data from normotensive and hypertensive humans. *Biomech Model Mechanobiol* 2011; 10: 867–882.

27. Taber LA. Biomechanics of growth, remodeling and morphogenesis. *Appl Mech Rev* 1995; 48: 487–545.

28. Donmazov S, Piskin S and Pekkan K. Noninvasive in vivo determination of residual strains and stresses. *J Biomech Eng* 2015; 137: 061011.

29. Sellier M. An iterative method for the inverse elasto-static problem. *J Fluid Struct* 2011; 27: 1461–1470.

30. Hirata K, Yaginuma T, O'Rourke MF, et al. Age-related changes in carotid artery flow and pressure pulses: possible implications for cerebral microvascular disease. *Stroke* 2006; 37: 2552–2556.

31. Verbeke F, Segers P, Heireman S, et al. Noninvasive assessment of local pulse pressure: importance of brachial-to-radial pressure amplification. *Hypertension* 2005; 46: 244–248.

32. Destrade M, Liu Y, Murphy JG, et al. Uniform transmural strain in pre-stressed arteries occurs at physiological pressure. *J Theor Biol* 2012; 303: 93–97.

33. Birger BI. *Temperature stresses in an anisotropic cylinder*. Washington: NASA, 1972.

Appendix 1

The determination of CCA pressure–radii waveform

During the US measurements, the blood pressure of the subject's left brachial artery (BrA) was continuously measured using an ABPI MD (MESI) device. The average diastolic and systolic BrA pressures were measured to be $P_{BrA}^d = 61.6\,\text{mmHg}$ and $P_{BrA}^s = 124.5\,\text{mmHg}$. The mean BrA pressure $\bar{P}_{BrA}$ was computed as $\bar{P}_{BrA} = P_{BrA}^d + 0.33(P_{BrA}^s - P_{BrA}^d)$.[30] Furthermore, by assuming that the mean and diastolic pressures are nearly constant throughout the large artery tree,[31] the CCA mean and diastolic pressures follow, being $\bar{P} = \bar{P}^{BrA}$ and $P^d = P_{BrA}^d$, respectively.

The CCA pressure waveform $P(t)$ can be obtained from the CCA radius waveform $r_i^{(M)}(t)$ by combining the diameter-derived pulse pressure method[17] and the exponential relationship between the arterial cross-sectional area and the pressure.[18,19] The functional relationship between the blood pressure waveform of the CCA $P(t)$ and the corresponding luminal cross-sectional area $A^{(M)}(t)$ as a function of time can be expressed as follows

$$P(t) = P^d \exp\left[\alpha_w\left(\frac{A^{(M)}(t)}{A^{d(M)}} - 1\right)\right] \quad (7)$$

with

$$\alpha_w = \frac{A^{d(M)}\ln(P^s/P^d)}{A^{s(M)} - A^{d(M)}}, A^{(M)}(t) = \pi\left(r_i^{(M)}(t)\right)^2 \quad (8)$$

where $A^{(M)}(t)$ was measured at the CCA location (M) (Figure 7(a)). $A^{d(M)}$ and $A^{s(M)}$ are the diastolic and systolic values of $A^{(M)}(t)$, P^s is the systolic pressure and α_w is the wall rigidity coefficient, which is pressure independent. The coefficient α_w was computed by an iterative scheme proposed by Meinders and Hoeks[18] based on the diastolic and mean CCA pressures, which was $\alpha = 1.21$. Finally, with α_w known, $P(t)$ and the CCA systolic pressure P^s follow from equation (7).

Determination of the pressure–radius waveform for segment (m). The luminal systolic area of the segment (m), designated as $A_i^{s(m)}$, was obtained from the outer systolic cross-sectional area $A_o^{s(m)}$ (represented with $A^{(m)}$ in Figure 7(a)). The time variation of the segment's cross section $A^{(m)}(t)$ is computed from equation (7) by assuming that the blood pressure $P(t)$ along the examined CCA section is constant $P(t)$.

Appendix 2

Mechanical response of a circular arterial segment

The principal stretches of a material particle in an arterial segment's loaded state are defined as follows

$$\lambda_r = \frac{\Theta_0 R}{\pi r \lambda \Lambda}, \lambda_\phi = \frac{\pi r}{\Theta_0 R}, \lambda_z = \lambda \Lambda \quad (9)$$

where λ_r, λ_ϕ and λ_z are the radial, circumferential and axial principal stretch, respectively, λ is the in vivo axial

stretch and Λ (which is normally being near unity) is the axial stretch associated with the longitudinal cut. In equation (9), all three successive motions of a particle (from Ω_0^C to the deformed configurations Ω_1^C, $\Omega_{1\lambda}^C$ or Ω_2^C, Figure 4(b)) are accounted for, where $r_i \leq r \leq r_o$, $r = r(t)$ and R corresponds to the material particle in the zero-stress configuration Ω_0^C. The deformation gradient tensor $\mathbf{F}$ can be written in terms of the principal stretches as $\mathbf{F} = \text{diag}[\lambda_r, \lambda_\phi, \lambda_z]$. The reference radius $R(r)$ can be determined by considering the incompressibility condition $J = \det \mathbf{F} = \lambda_r \lambda_\phi \lambda_z = 1$ as follows

$$R = \left(R_o^2 - \frac{\pi \lambda \Lambda}{\Theta_0} \left(r_o^2 - r^2 \right) \right)^{\frac{1}{2}} \tag{10}$$

For an isotropic incompressible material, the Cauchy stress tensor $\boldsymbol{\sigma}$ is given by

$$\boldsymbol{\sigma} = -p\mathbf{I} + \bar{\boldsymbol{\sigma}} = -p\mathbf{I} + 2\mathbf{F}\frac{\partial W}{\partial \mathbf{C}}\mathbf{F}^{\mathrm{T}} \tag{11}$$

where p is the Lagrange multiplier that enforces incompressibility and $\mathbf{I}$ is the identity tensor. The non-zero components of the stress tensor follow using relation (9) and the strain energy density function W, equation (5), as follows

$$\sigma_{kk} = -p + \bar{\sigma}_{kk} = -p + \lambda_k^2 c_a$$
$$\exp\left[\frac{c_b}{2}\left(\lambda_r^2 + \lambda_\phi^2 + \lambda_z^2 - 3\right)\right]; \quad k = r, \phi, z \tag{12}$$

where $\sigma_{kk} = \sigma_{kk}(r,t)$; $k = r, \phi, z$ and $p = p(t)$. The Lagrange multiplier p can be obtained by solving the given boundary value problem. In the absence of body forces, and by treating the problem as quasi-static,[21] the equation of motion reduces to the following

$$\frac{\mathrm{d}\sigma_{rr}}{\mathrm{d}r} + \frac{\sigma_{rr} - \sigma_{\phi\phi}}{r} = 0 \tag{13}$$

The associated boundary conditions depend on the blood pressure $P(t)$, whereas the outer surface is considered traction-free

$$\sigma_{rr}(r_i, t) = -P(t), \quad \sigma_{rr}(r_o, t) = 0 \tag{14}$$

The Lagrange multiplier can be obtained from equation (13) using the boundary conditions given by relation (14), which is as follows

$$p = P^{CA} + \bar{\sigma}_{rr} - \int_{r_i}^{r} (\sigma_{\phi\phi} - \sigma_{rr}) \frac{\mathrm{d}r}{r} \tag{15}$$

In addition, the fulfilment of the equilibrium in the configuration in vivo requires the following

$$\int_{r_i}^{r_o} (\sigma_{\phi\phi} - \sigma_{rr}) \frac{\mathrm{d}r}{r} = P^{CA} \tag{16}$$

The stretched-state geometry of the segment $\Omega_{1\lambda}^C$ (Figure 4(b)), with the material particles positioned in the interval $\rho_i \leq \rho \leq \rho_o$, is obtained from the above equations by considering the traction-free boundary condition on both the inner and outer surface of the segment.

Identification problem. Because the in vivo data (i.e. the pressure–radius cycle) are insufficient to determine the identification variables,[22] the following assumptions are adopted: (1) the axial stretch λ is independent of blood pressure,[22] (2) the ratio between circumferential and axial stress κ is known for one (arbitrary) value of blood pressure[22] and (3) the transmural gradient of the circumferential stretch λ_ϕ is homogeneous at the mean blood pressure,[32] which takes into account the uniform strain hypothesis.[7] The stress ratio κ is taken from Masson et al.[26] in which circular CCA segments from seven young subjects were characterised (their ages ranged from 21 to 42 years, the average being 31.8 years). The average value of the ratio $\kappa = \sigma_{\phi\phi}/\sigma_{zz}$, which corresponds to the segment's outer diastolic radius, is $\kappa \approx 1.9$.

The unknowns of the segment (M) that need to be determined are $\boldsymbol{u} = \{R_o^{(M)}, \Theta_0^{(M)}, c_a, c_b\}$, represented with the optimization vector $\boldsymbol{u}$. We define the objective function χ to account for (1) the difference between the computed and measured blood pressure (Figure 7(b)), (2) the ratio between the circumferential and axial stresses and (3) the uniform strain hypothesis, represented by the first, second and third terms in equation (17)

$$\chi(\boldsymbol{u}) = \sum_{i=1}^{N} \left[\left(P_i^{\text{th}}(\boldsymbol{u}) - P_i \right)^2 \right] + g_\sigma \left(\frac{\sigma_{\phi\phi}^{d,o}(\boldsymbol{u})}{\sigma_{zz}^{d,o}(\boldsymbol{u})^{-\kappa}} \right)^2$$
$$+ g_\lambda \left(\lambda_\phi^i(\boldsymbol{u}) - \lambda_\phi^o(\boldsymbol{u}) \right)^2 \tag{17}$$

In relation (17), N is the number of data points, P_i^{th} is the computed intraluminal pressure, λ_ϕ^i and λ_ϕ^o are the circumferential stretches computed for the inner and outer surfaces of the segment's wall, respectively, and $\sigma_{\phi\phi}^{d,o}$ and $\sigma_{zz}^{d,o}$ are the systolic circumferential and the axial, respectively.

Appendix 3

TM circular segment

Temperature field of the circular TM segment. The TM model is exposed to a temperature change applied to its inner and outer surfaces (Figure 4(c)). The initial temperature of the segment is assumed to be uniform and

is set to 0. Adiabatic boundary conditions are applied to the front and rear surfaces of the fictitious model.

The temperature distribution T, where $T = T(r)$, is computed from the following relation

$$T(r) = \Delta T_i + \frac{\Delta T_o - \Delta T_i}{\ln(r_o/r_i)} \ln\left(\frac{r}{r_i}\right) \quad (18)$$

This is obtained by solving the steady-state heat equation and assuming for the boundary conditions thermal loads ΔT_i and ΔT_o, which are applied to the segment's inner and outer surfaces, where $r_i = r_o - \delta^\Psi$.

TM response of the segment. For a transversely isotropic elastic material, the fourth-order **D** elasticity tensor is written as follows

$$\mathbf{D} = \begin{bmatrix} 1/E_P^\Psi & -\nu_P/E_P^\Psi & -\nu_{TP}/E_T^\Psi & 0 & 0 & 0 \\ -\nu_P/E_P^\Psi & 1/E_P^\Psi & -\nu_{TP}/E_T^\Psi & 0 & 0 & 0 \\ -\nu_{PT}/E_P^\Psi & -\nu_{PT}/E_P^\Psi & 1/E_T^\Psi & 0 & 0 & 0 \\ 0 & 0 & 0 & 1/G_P^\Psi & 0 & 0 \\ 0 & 0 & 0 & 0 & 1/G_T^\Psi & 0 \\ 0 & 0 & 0 & 0 & 0 & 1/G_T^\Psi \end{bmatrix}$$

and $G_P^\Psi = E_P^\Psi/(2(1+\nu_P))$.[14] Thermal stresses caused by the temperature change $T(r)$ can be obtained from linear elasticity. For a transversely isotropic material behaviour, the following relations are obtained[33]

$$\sigma_{rr} = A_P \frac{du}{dr} + A_{PT}\frac{u}{r} + A_{TP}e - \beta_P T$$

$$\sigma_{\phi\phi} = A_{PT}\frac{du}{dr} + A_P\frac{u}{r} + A_{TP}e - \beta_P T$$

$$\sigma_{zz} = A_{TP}\left(\frac{du}{dr} + \frac{u}{r}\right) + A_T e - \beta_T T \quad (19)$$

$$\sigma_{r\phi} = \sigma_{rz} = \sigma_{\phi z} = 0$$

where $u(r)$ is the radial displacement and

$$A_P = \frac{E_P^\Psi(1-\nu_{TP}\nu_{PT})}{D} \qquad D = 1 - 2\nu_P\nu_{TP}\nu_{PT} - 2\nu_{TP}\nu_{PT} - \nu_P^2$$
$$A_{PT} = \frac{E_P^\Psi(\nu_P + \nu_{TP}\nu_{PT})}{D} \qquad \beta_P = A_P\alpha_P + A_{PT}\alpha_P + A_{TP}\alpha_T$$
$$A_{TP} = \frac{E_P^\Psi(\nu_{TP} + \nu_P\nu_{TP})}{D} \qquad \beta_T = 2A_{TP}\alpha_P + A_T\alpha_T$$
$$A_T = \frac{E_T^\Psi(1-\nu_P^2)}{D}$$
$$(20)$$

The TM response of a segment is then obtained by solving the set of two first-order differential equations for $u(r)$ and $\sigma_{rr}(r)$[33]

$$\frac{du}{dr} = -\frac{A_{PT}}{A_P}\frac{u}{r} + \frac{\sigma_{rr}}{A_P} - \frac{A_{TP}}{A_P}e + \frac{\beta_P}{A_P}T$$

$$\frac{d\sigma_{rr}}{dr} = \left(A_P - \frac{A_{PT}^2}{A_P}\right)\frac{u}{r^2} + \left(\frac{A_{PT}}{A_P} - 1\right)\frac{\sigma_{rr}}{r} \quad (21)$$

$$+ \left(A_{TP} - \frac{A_{PT}A_{TP}}{A_P}\right)\frac{e}{r} + \left(\frac{A_{PT}}{A_P} - 1\right)\frac{\beta_P T}{r}$$

where traction-free boundary conditions on both inner and outer surfaces of the segment are considered. Afterwards, the remaining non-zero components of the stress tensor follow from relations (19).

Identification problem. The unknown properties of the circular TM segments (m) and (M) are determined by solving a minimization problem. The goal of the problem is for the TM segment's loaded state $\Psi_{1\lambda}^C$ (more precisely, its geometry and stresses) to match the stretched state of its corresponding arterial segment $\Omega_{1\lambda}^C$ (Figure 4(b)).

The objective function $\chi = \chi(v)$, where v is the vector of the optimization variables $v = (E_P^\Psi, \alpha_P, E_T^\Psi, \alpha_T, \delta^\Psi, \Delta T_i, \Delta T_o)$, is formulated to account for (1) the relative error between the computed geometry of the fictitious segment and the desired geometry and (2) the relative error between the computed and desired stress states. χ is thus written as follows

$$\chi(v) = \sum_{m=r,\phi,z} \frac{1}{N_m} \sum_{k=1}^{N_m} \left(\frac{S_{ck}^m(v) - S_k^m}{S_k^m}\right)^2$$

$$+ g_\rho \sum_{k=i,o} \left(\frac{\rho_k^\Psi(v) - \rho_k}{\rho_k^\lambda}\right)^2 \quad (22)$$

where vectors $\mathbf{S}_c^m$ and $\mathbf{S}^m$; $m \in \{r, \phi, z\}$ hold the computed and desired discrete values of the radial, circumferential and axial stresses (note that in $\mathbf{S}^m$, only the non-zero values of the stresses are considered), respectively, while N_m; $m \in \{r, \phi, z\}$ is the length of vector $\mathbf{S}^m$. The quantities ρ_k^Ψ and ρ_k; $k \in \{i, o\}$ are the inner and outer radii of the TM (computed) and arterial (desired) segment, respectively, and g_ρ is the weighting factor.

The identification procedure was first performed for the TM segment (M). Then, by adopting E_P^Ψ, α_P and E_T^Ψ, the identification of parameters for the segment (m) followed.